International Conference on Textile Composites and Inflatable Structures
STRUCTURAL MEMBRANES 2011
E. Oñate, B. Kröplin and K.-U.Bletzinger (Eds)

FINITE ELEMENT ANALYSIS ON MULTI-CHAMBER TENSAIRITY-LIKE STRUCTURES FILLED WITH FLUID AND/OR GAS

ANNE MAURER*, ALEXANDER KONYUKHOV AND KARL SCHWEIZERHOF

*Institut für Mechanik
Karlsruhe Institute of Technology (KIT)
76128 Karlsruhe, Germany
e-mail: info@ifm.kit.edu, www.ifm.kit.edu

Key words: Fluid-Structure Interaction, Contact, Cable, Tensairity, Finite Element

Abstract. The concept of Tensairity-structures [6] developed by the company Airlight in Biasca, Switzerland, has been known since 2004. The advantages of the airbeams with a compression element and a spiraled cable are essentially their light weight and that such beams can be used for wide span structures.
To achieve a further weight reduction Pronk et al [8] proposed to replace the compression element by an additional slim chamber filled with water. Experiments with these multi-chamber beams with and without cables showed a stiffer behavior in bending tests compared to only air filled beams.
In the current contribution different tests like - primarily - the bending of multi-chamber beams will be simulated with finite elements. Explicit and implicit finite element simulations with LS-DYNA [7] and FEAP-MeKa [11] respectively will be performed with a special focus on the interaction of structural deformations and the gas/fluid filling in combination with the cables contacting the membranes. The specific features have been implemented in the above codes.
The fluid and/or gas filling is replaced by an energetically equivalent load and corresponding stiffness matrix contributions to simulate quasi-static fluid-structure interaction taking the effect of the deformations of the chambers on the fluid/gas filling into account. This approach has already been introduced for fluid-structure interaction problems with large deformations and stability analysis in [1], [2]. For the implicit simulation the cables will be added using special solid-beam finite elements [5]. A new curve-to-surface contact algorithm is developed to model the contact interaction between cables and the deformable shell structure.

1 INTRODUCTION

Structures filled with fluid and/or gas combined with cables can be found in various fields, for example in balloons, airbags, pipeline buoyancy or water load test weights, airbeams and waterbeams. In all of these examples the filling proceeds quasi-statically, thus the fluid can be described by an energetically equivalent loading. The algorithms based on the theory of quasi-static fluid-structure interaction are implemented in LS-Dyna [7] for explicit and in FEAP-MeKa [11] for implicit finite element simulations and have already been presented for many examples, see [1], [2], [7]. Cables can be modeled by special solid-beam finite elements [5] and a curve-to-surface contact algorithm. The combination of both is applied to airbeams and waterbeams, which consist of one or more fluid filled chambers wrapped with cables.

2 QUASI-STATIC FLUID-STRUCTURE INTERACTION

During the filling of airbeams and waterbeams dynamic behavior is not expected because of a slow, quasi-static filling process. As a result the effect of gas or water inside a chamber can be described by an energetically equivalent pressure load vector and also the standard water loading is quasi static. Both are also leading to corresponding striffness contributions. An important aspect is that the water/gas loading is defined via given initial volumes and gas or fluid deformation relations. This is predominantly important for structures undergoing large deformations or in stability prone problems.
Of course this idea can not only be applied to airbeams and waterbeams. Other structures including quasi static fluid structure interaction are e. g. hydro-forming, buoyancy simulation of ships and inflatable dams.
In the following subsections all three different load-cases (pure gas loading, incompressible fluid loading and incompressible fluid with compressible gas loading) are discussed. A complete derivation and further load cases considering also compressible fluid can be found in [3] and [9].

2.1 Gas

In case of gas loading the whole internal boundary of a gas filled chamber is loaded with a constant gas pressure p^g.
As shown in Figure 1 p^g is the gas pressure, $\partial\Omega^g$ the boundary and $\mathbf{n}^g$ the normal directed towards the outside of the wetted structure. The virtual work term resulting in a load vector due to gas loading, which has to be added to an arbitraray structural load vector, reads as

$$\delta\Pi^g_{ext} = \int_{\Omega^g} p^g \mathbf{n}^g \cdot \delta\mathbf{u}^g \mathrm{d}\Omega^g \tag{1}$$

with the variation of the displacement $\delta\mathbf{u}^g$.

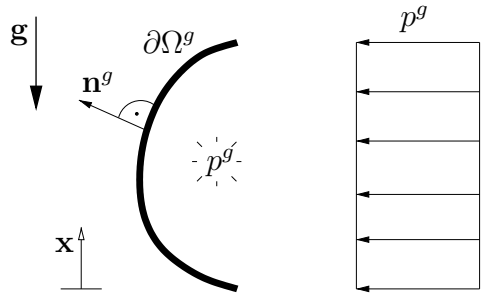

Figure 1: Pressure in a gas filled chamber

After each time step the gas pressure has to be updated considering a simple gas law with the adiabatic exponent κ and the gas volume v^g:

$$p^g = p^g_{old} - \kappa p^g_{old} \frac{v^g - v^g_{old}}{v^g_{old}}. \tag{2}$$

The pressure is hereby as in the following load cases controlled by volume modifications.

2.2 Incompressible Fluid

Without an additional gas loading there is a free fluid surface and the following load case is achieved considering only incompressible fluid as the compressibility of the fluid plays no role in the rather soft structure considered in this contribution.

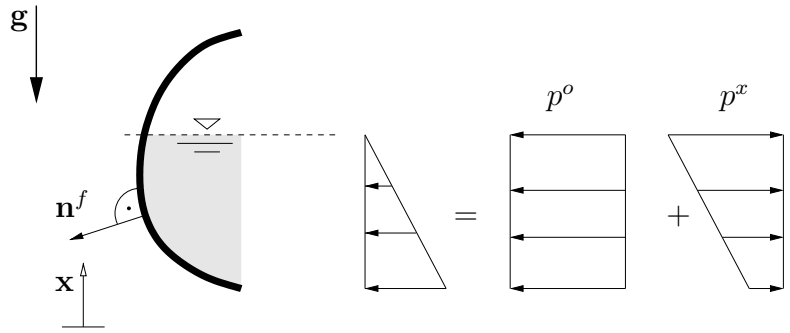

Figure 2: Hydrostatic pressure in a partially filled chamber

With the gravity vector $\mathbf{g}$, the outward directed normal of the wetted surface $\mathbf{n}^f$, the density of the fluid ρ and the coordinate to the fluid surface $\mathbf{x}^o$ the pressure at water level is computed by

$$p^o = \rho \mathbf{g} \cdot \mathbf{x}^o \tag{3}$$

and the pressure at any point of the wetted surface is

$$p^x = \rho \mathbf{g} \cdot \mathbf{x} \qquad\qquad \mathbf{x} = \mathbf{0} \ldots \mathbf{x}^o. \tag{4}$$

This leads to the virtual work of a load vector consisting of p^x and p^o:

$$\delta\Pi^f_{ext} = \int_{\Omega^f} (p^x - p^o)\mathbf{n}^f \cdot \delta\mathbf{u} \, \mathrm{d}\Omega^f. \tag{5}$$

2.3 Incompressible Fluid combined with Gas

The last presented load case is the combination of the two previous load cases.

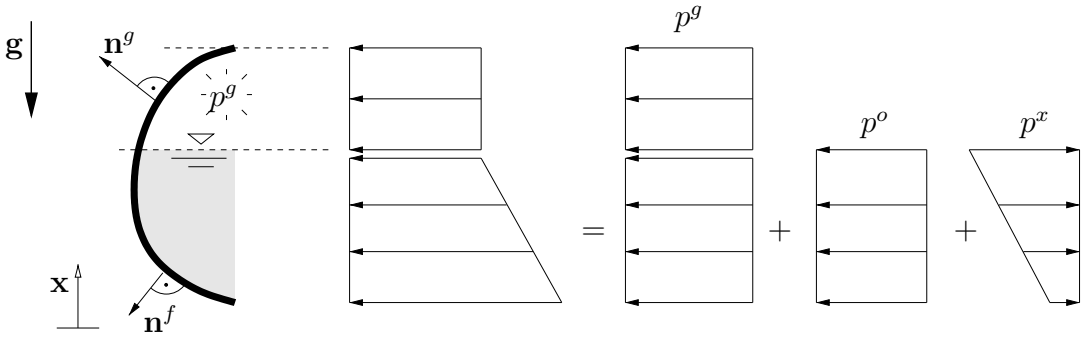

Figure 3: Hydrostatic pressure of a fluid and gas filled chamber

The virtual work of the load vector is a combination of equation (1) and (5):

$$\delta\Pi^f_{ext} + \delta\Pi^g_{ext} = \int_{\Omega^f} (p^g + p^x - p^o)\mathbf{n}^f \cdot \delta\mathbf{u} \, \mathrm{d}\Omega^f + \int_{\Omega^g} p^g \mathbf{n}^g \cdot \delta\mathbf{u} \, \mathrm{d}\Omega^g \tag{6}$$

The update of the gas pressure is performed in analogy to equation (2) in the case of only gas loading.
The last two cases and an extension to multiple chambers have been implemented into LS-DYNA following a previous implementation in FEAP-MeKa [11], [10], [3]. For the further theoretical background and its implications for implicit algorithms we refer to [10], [3], [1].

3 CABLES AND CONTACT

Several developments are required to obtain a robust contact algorithm for cable and shell interactions: robust shell finite elements, robust cable finite elements and contact algorithms for the cable-shell interaction. Shell finite element technology is highly developed and a wide range of various formulations is available. Here we are selecting the solid-shell finite element with only displacement degrees of freedoms. For the cable we take a special solid-beam finite element with exact representation of an elliptical cross-section, see in [5].

3.1 SOLID-BEAM FINITE ELEMENT

The solid-beam element is constructed as follows, see Fig. 4: a) the mid-line of the beam is taken, first, with e.g. linear approximation. It is defined then by nodes 1 and 2; b) the left cross-section is defined to be elliptic with the reference main axes defined by nodes 1-3 and 1-4; c) the right cross-section is defined to be elliptical with the reference main axes defined by nodes 2-5 and 2-6. This element allows an iso-geometrical description of the elliptic cross-section, in- and out of plane deformations of this cross-section together with tension type rotations of the cross-section along the mid-line and bending. the element can be easily extended into an iso-geometric spline-element along the mid-line.

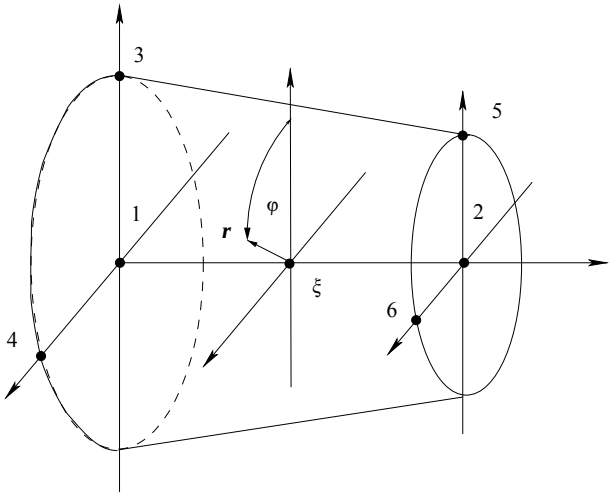

Figure 4: "Solid-Beam" with elliptical cross-sections defined by 6 nodes. Definition of local variables.

A special set of shape functions defining iso-geometrically an elliptical shape of the cross-section is exploited. The mid-line can be also represented by e.g. NURBS or other spline functions following the iso-geometric approach.

3.2 CURVE-TO-SURFACE CONTACT ALGORITHM

The kinematics of the curve-to-surface contact element is dually defined, first, in the Serret-Frenet coordinate system following the curve-to-curve contact algorithm developed in [5], and, second, in the surface coordinate system following the covariant description in [4]. This leads in the case of linear approximations for both shells and ropes to the following 6-nodes curve-to-surface (CTS) contact element, see Fig. 5, which is constructed as follows: i) the shell surface (in this case linearly approximated) is covered by the master contact segments with nodes $1, 2, 3, 4$; ii) for the contact definition the mid-line represented by nodes $5, 6$ of the solid-beam element is taken; iii) contact kinematics is defined in the local coordinate system attached to the master segment with coordinate vectors $\boldsymbol{\rho}_1, \boldsymbol{\rho}_2, \mathbf{n}$, see more in [5], however, assuming representing the coordinate system attached to the

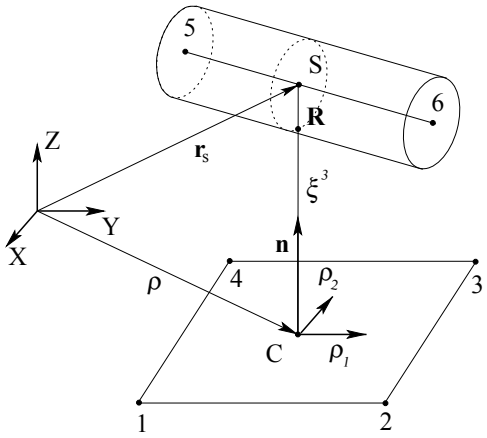

Figure 5: Kinematics of the Curve-To-Surface contact element.

line.

$$\mathbf{r}_s(\eta, \xi^1, \xi^2) = \boldsymbol{\rho}(\xi^1, \xi^2) + \mathbf{n}(\xi^1, \xi^2)\xi^3, \tag{7}$$

where ξ^1, ξ^2 are convective coordinates for the master segment and η is a convective coordinate for the mid-line of the slave solid-beam element. iv) penetration ξ^3 is computed assuming the thickness of the rope as between the distance between the integration point on the mid-line S and its projection on the surface C subtracting the radius of the rope R. It leads in the case of the circular cross section with radius R to the following expression:

$$\xi^3 = (\mathbf{r}_s - \boldsymbol{\rho}) \cdot \mathbf{n} - R. \tag{8}$$

v) The contact integral is computed numerically using the integration formulae of Lobatto or Gauss type depending on modeling purposes. The part responsible for normal contact only is represented by

$$\delta W = \int_{5-6} N \delta \xi^3 ds_{5-6} \tag{9}$$

vi) in the case of the penalty regularization the normal force is computed as $N = \varepsilon_N \xi^3$ with ε_N as a penalty parameter

4 AIRBEAM

Tensairity-structures have been developed by Airlight in 2004 [6]. These light-weight structures consist of a gas filled fabric structure with a compression element and a spiraled cable. The inflation process for airbeams and most of the loading proceeds quasi-statically, so that the theory in section 2 can be applied without any restriction.
For the finite-element simulation the fabric structure is designed like a cylinder with radius of $0,23m$ and a length of $2m$ and was model with shell elements, see Figure 6. The thickness of the material is $1mm$. The width of the compression element is $0,1m$ with a thickness of $0,01m$ and consists of volume elements. In all simulations gravity was added.

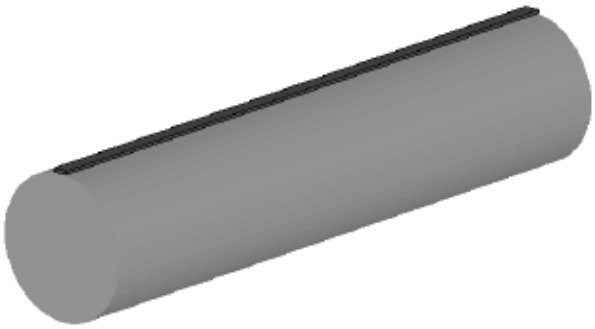

Figure 6: Initial configuration for airbeam simulation without cables

In the finite element simulations the airbeams were filled with gas varying the gas pressure from 1 bar to 40 bar. After the inflation process the center line of the compression element was loaded in transverse direction with a linearly increasing force F. The deformation of the airbeam after inflation caused by the force F was measured.

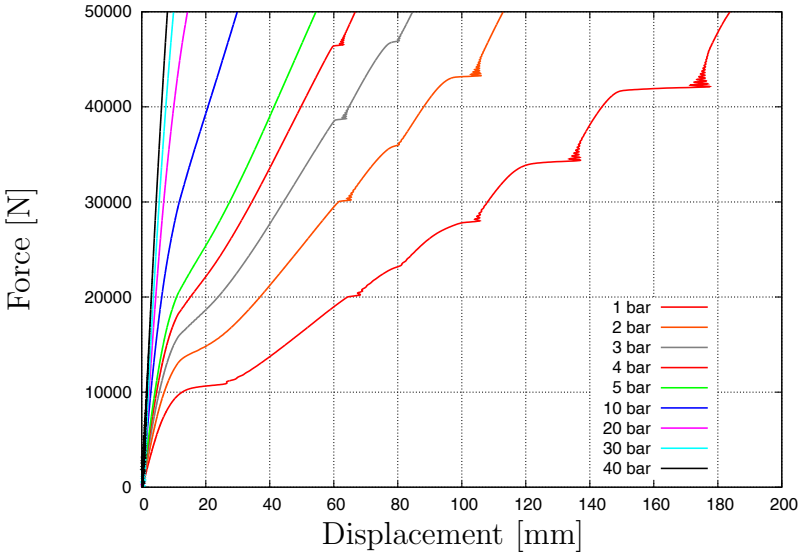

Figure 7: Initial configuration for airbeam simulation without cables

As expected the displacement decreases with a higher gas pressure. Especially the deformations of an airbeam filled with atmospheric pressure of 1 bar are very large. Further investigations with cables - currently underway - should show less deformations even for the low pressure cases.

5 WATERBEAM

The concept of waterbeams, see [8], is a further development of the airbeam. Instead of a stable compression element an additional membrane chamber is included. This chamber is as long as the waterbeam itself, but the radius is much smaller, see chamber 2 in Figure 8 and can be filled with gas or fluid. The larger chamber 1 is filled with gas. A vertical continuous membrane divides chamber 1 to accommodate the shear force. On the left and right end of the waterbeam the beam is fixed to two round steel plates.

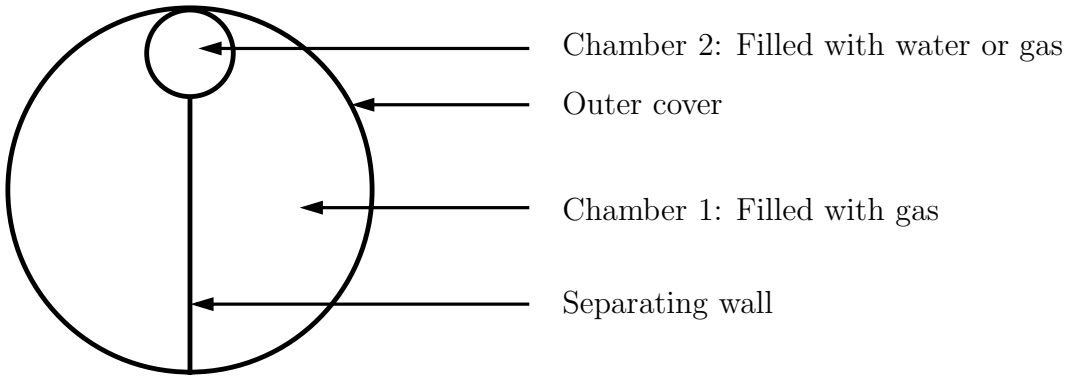

Figure 8: Cross-section of waterbeam

The radius of chamber 2 is $3cm$ and the larger radius of chamber 1 is $23cm$. In total the waterbeam has a length of $2m$ which includes the steel plates. The thickness of the membrane was again set to $1mm$. In the finite element simulation the membrane chambers are discretized with 50000 shell elements, and the cables are discretized with 500 beam elements in LS-Dyna. Youngs modulus of the membrane material is $7,6 \cdot 10^9 Pa$, density $1kg/m^3$.

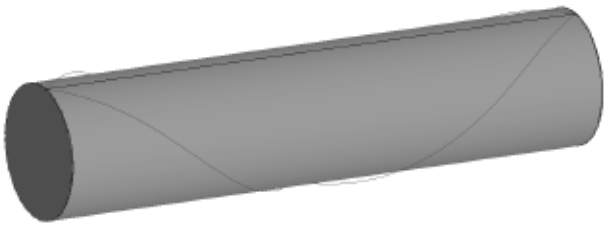

Figure 9: Initial configuration for waterbeam simulation

In a first simulation the waterbeam was loaded only with fluid to verify the multi-chamber approach in the finite element simulation. While chamber 1 is always filled with a gas

pressure of 1 bar, the second chamber is once filled with gas (gas pressure 1 bar) and in a second simulation filled with fluid (water height $0,23m$).

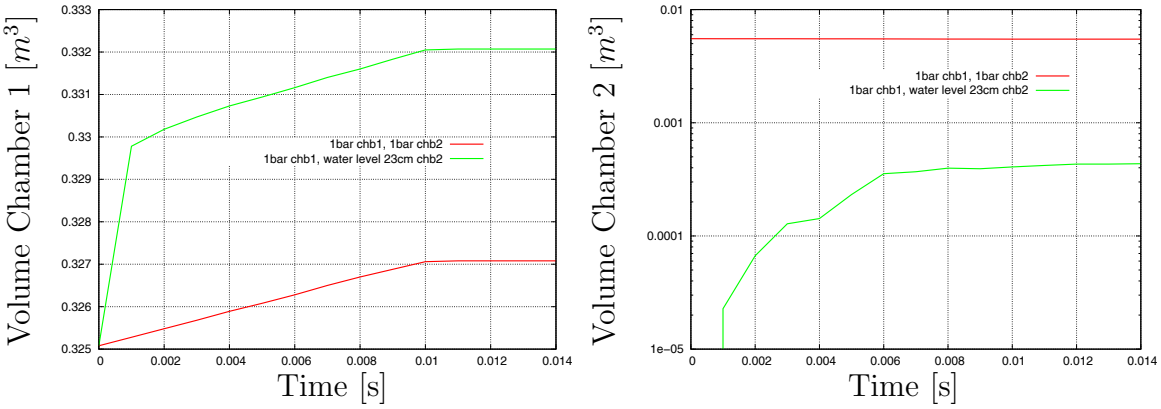

Figure 10: Gas and Fluid volume for chamber 1 and chamber 2 with different types of fluid loading

Both the fluid and the gas loading are applied until a maximum at time $0,01s$. In case of the water filling in chamber 2 the water is added a little bit later than the gas filling of chamber 1. This results in a slightly higher gas volume in chamber 1 and lower fluid volume in chamber 2.
In further simulations -currently underway - the waterbeam will be transversely loaded with a force F in the middle of chamber 2 and the deformations will be measured. A result analogously as in Figure 7 is expected.
First simulations with cables using LS-Dyna show the filling process and the contact with cables during the filling process, see Figure 11.

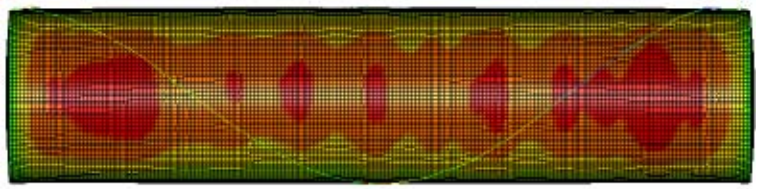

Figure 11: Waterbeam with cables during filling process showing the displacement

6 CONCLUSIONS

Light-weight structures like airbeams are already used for bridges, for example in the Ski resort Val-Cenis. The newer concept of waterbeams developed by [8] has been simulated to compare the deformation to the deformations of a airbeam with identical loading.

For both concepts quasi-static fluid-structure interaction can be applied. The cable was simulated as a beam structure. In FEAP-MeKa, [11], a newly developed cable formulation could be used while in LS-Dyna a standard beam formulation was used to simulate the cables. In a first step the airbeam structure was simulated without cables. Deformations due to a force F increase with an decreasing gas pressure. For the example of a waterbeam multi-chamber fluid-structure interaction has been used. The results of displacement simulations with a force F as well as the comparison to the experimental results in [8] will be shown at the Structural Membranes 2011 conference.

REFERENCES

[1] Haßler, M. and Schweizerhof, K. On the static interaction of fluid and gas loaded multi-chamber systems in a large deformation finite element analysis. *Comp. Meth. Appl. Mech. Engrg.* (2008) **197**:1725–1749.

[2] Haßler, M. and Schweizerhof, K. On the influence of fluid-structure interaction on the static stability of thin walled shell structures. *Int. J. Struct. Stab.* (2007) **7**:313–335.

[3] M. Haßler: Quasi-Static Fluid-Structure Interactions Based on a Geometric Description of Fluids. Dissertation, Institut für Mechanik, Universität Karlsruhe (TH), 2009.

[4] Konyukhov, A. Geometrically Exact Theory for Contact Interactions, *Habilitationsschrift*, Karlsruhe, KIT, 2010.

[5] Konyukhov A., Schweizerhof K. Geometrically exact theory for contact interactions of 1D manifolds. Algorithmic implementation with various finite element models. *Comput. Method. Appl. Mech. Engrg.* available online April 2011, doi:10.1016/j.cma.2011.03.013.

[6] Luchsinger, R.H. et al.. Going strong: From inflatable structures to Tensairity. *Textile Composits and Inflatable Structures II* CIMNE, Barcelona, 414–420 (2005).

[7] Maurer A. Gebhardt, M. and Schweizerhof, K. Computation of fluid and/or gas filled inflatable dams. LS-Dyna Forum, Bamberg, Germany (2010).

[8] Pronk, A. and Maffei, R. and Martin, H. Research on the combination of water and membranes as a structural building material. *Proceedings of the IASS Symposion*, Valencia (2009).

[9] T. Rumpel and K. Schweizerhof: Hydrostatic fluid loading in non-linear finite element analysis. *Int. J. Num. Meth. Engrg.* (2004) **59**: 849–870.

[10] T. Rumpel: Effiziente Diskretisierung von statischen Fluid-Struktur-Problemen bei großsen Deformationen. Dissertation, Institut für Mechanik, Universität Karlsruhe (TH), 2003.

[11] Schweizerhof, K. et al. FEAP-MeKa, Finite Element Analysis Program, Karlsruhe Institute of Technology, based on Version 1994 of R. Taylor, FEAP – A Finite Element Analysis Program, University of California, Berkeley, 2011.